


NANO EXPRESS

Open Access



# Integration of Environmental Friendly Perovskites for High-efficiency White Light-emitting Diodes

Hanxin Liu, Chun Sun<sup>\*</sup> , Zhiyuan Gao, Chong Geng, Shuangshuang Shi, Le Wang, Sijing Su and Wengang Bi<sup>\*</sup>

## Abstract

Perovskite quantum dots (QDs) have been widely used in white light-emitting diodes (WLEDs), due to their high quantum yield (QY), tunable bandgap, and simple preparation. However, the red-emitting perovskite QDs are usually containing iodine (I), which is not stable under continuous light irradiation. Herein, perovskite-based WLED is fabricated by lead-free bismuth (Bi)-doped inorganic perovskites  $\text{Cs}_2\text{SnCl}_6$  and less-lead Mn-doped  $\text{CsPbCl}_3$  QDs, which emits white light with color coordinates of (0.334, 0.297). The Bi-doped  $\text{Cs}_2\text{SnCl}_6$  and Mn-doped  $\text{CsPbCl}_3$  QDs both show excellent stability when kept in the ambient air. As benefits from this desired characteristic, the as-prepared WLED shows excellent stability along with operating time. These results can promote the application of inorganic perovskite QDs in the field of WLEDs.

**Keywords:** Quantum dots, perovskite, WLED, doping

## Introduction

Among solid-state lighting technology, white light-emitting diodes (WLEDs) are excellent candidates to replace incandescent lamps for their merits of high-energy conservation, long lifetime, high luminous efficiency, and polarized emissions [1]. In general, WLEDs were recognized as one kind of the economical and efficient solid-state lighting sources [2, 3]. QD-LED technology is gradually developed over the past few years, because of high stability and high quantum yield (QY) of quantum dots (QDs) [4]. Recently, perovskites have attracted much attention, and they have been applied in many different fields [5–15]. Perovskite solar cells with power conversion efficiency (PCE) exceeding 23% have been achieved because of their excellent absorption (Abs) coefficients, long carrier diffusion lengths, and high carrier mobilities [5–7].  $\text{CsPbBr}_3$ -encapsulated PbSe wires have shown good optoelectronic performance including high responsivity ( $\sim 10^4 \text{ A W}^{-1}$ ) and fair response speed ( $\sim \text{ms}$ ), demonstrating their great potential application in photodetection fields [8–10]. Additionally, perovskites have been introduced into photonic devices. The remarkable features of perovskite,

such as rich phase compositions and low-temperature solution process ability, made perovskite can be applied in transistors [5]. Low-threshold amplified spontaneous emission and lasing can be realized by  $\text{CsPbX}_3$  QDs [11]. Most of all, perovskite QDs are the most promising material among QDs for LED application, due to high QY (up to > 90%), intense photoluminescence (PL), simple preparation procedure, and highly tunable bandgaps (from 1.46 to 2.50 eV) [11–16]. However, the anion-exchange reaction between perovskites and instability of iodine (I)-containing perovskite largely restricted the development of perovskite QDs toward WLED application. Sun et al. proposed to use silica encapsulation to enhance stability and avoid anion exchange [17]. The air stability of perovskite QDs was enhanced greatly, but the WLED stability is not good enough because of the significant dropping of red light. Then, Shen et al. used the anthracene shell to protect red-emitting perovskite QDs, which enhanced the LED stability against current [18]. Zhong and coworkers directly used red-emitting  $\text{K}_2\text{SiF}_6:\text{Mn}^{4+}$  phosphor to replace iodine (I)-containing perovskite QDs [19]. Sun and coworkers also presented the same method to enhance the stability of LED [20]. Due to the sharp emission lines of perovskite QDs, they usually are used in backlight display application with blue-emitting LED chips [21, 22]. These WLEDs are not proper for solid-state lighting, because their

\* Correspondence: [cs@hebut.edu.cn](mailto:cs@hebut.edu.cn); [wbi@hebut.edu.cn](mailto:wbi@hebut.edu.cn)  
Tianjin Key Laboratory of Electronic Materials and Devices, School of Electronics and Information Engineering, Hebei University of Technology, 5340 Xiping Road, Tianjin 300401, People's Republic of China

CRI is quite low. Recently, several reports have prepared single-phase phosphor of perovskites, which possess broad linewidths. However, the QYs of this kind of material are relatively low [23–25]. Another great problem is that the perovskite QDs contain lead, which is poison to health and environment [26, 27]. With the growing concerns about this risk, restrictions have been made to limit the use of Pb in consumer electronics. A lot of efforts have been done to explore and replace lead with less toxic elements like Sn, Ge, Bi, and Sb, which have analogous electronic band structure [28–30]. However, their optoelectronic properties cannot be comparable with the Pb-based counterparts. Doping less toxic elements into perovskite lattice has been an alternative route, which can introduce new optical, electronic, and magnetic properties [31, 32]. For example, Zhang et al. have prepared Mn-doped perovskite QDs with QYs up to 54% and the highest Mn substitution ratio was 46% [31]. Tang and co-workers reported Bi-doped lead-free inorganic perovskites. After doping Bi, the PLQY of Bi-doped  $\text{Cs}_2\text{SnCl}_6$  is enhanced to 78.9% [33].

In this work, we introduce Mn-doped  $\text{CsPbCl}_3$  QDs and Bi-doped  $\text{Cs}_2\text{SnCl}_6$  as the orange emission light and blue emission light to fabricate high-performance WLEDs. These two materials both can be excited by UV light and exhibit high QYs under UV light. They also contain the same anion Cl, which avoids the anion exchange reaction during the mixing process. Besides, it is worth to note that the emission linewidths of these two perovskites are very broad, which facilitate to form a continuous spectrum. In a WLED with a CCT of 5311K, the color coordinates of (0.334, 0.297) and CRI of 80 were achieved. Most of all, this WLED showed excellent stability against increasing currents and working time.

## Methods

### Materials and Chemicals

Cesium carbonate ( $\text{Cs}_2\text{CO}_3$ , 99.9%), lead (II) chloride ( $\text{PbCl}_2$ , 99.999%), cesium chloride ( $\text{CsCl}$ , 99.99%), oleic acid (OA, 90%), and 1-octadecene (ODE, 90%) were obtained from Alfa Aesar. Manganese chloride tetrahydrate ( $\text{MnCl}_2(\text{H}_2\text{O})_4$ , 99.99%), oleylamine (OAm, 80–90%), and tin chloride ( $\text{SnCl}_2$ , 99.99%) were purchased from Aladdin. Bismuth chloride ( $\text{BiCl}_3$ , 99.99%) and polymethyl methacrylate (PMMA) were obtained from Macklin. Hydrochloric acid (HCl, 37 wt.% in water) was purchased from Sinopharm Chemical Reagent Co., Ltd. Methanol (99.5%) was obtained from Kermel. Toluene (99.0%) and ethyl acetate (99.5%) were purchased from Concord. Hexane was obtained from Beijing Chemical Factory.

### Synthesis Processes

**Preparation of Cs-oleate** The cesium-oleate solution was prepared according to the approach by Kovalenko

and co-workers [31]. In brief, 0.8 g of  $\text{Cs}_2\text{CO}_3$ , 2.5 mL of OA, and 30 mL of ODE were loaded in a three-neck flask and dried under vacuum at 120 °C for 1 h. Next, the flask was switched to  $\text{N}_2$  atmosphere and heated to 150 °C until all the  $\text{Cs}_2\text{CO}_3$  dissolved.

**Synthesis of Mn-doped  $\text{CsPbCl}_3$**  The Mn-doped  $\text{CsPbCl}_3$  was synthesized by hot injection method. Typically, 0.0615 g of  $\text{PbCl}_2$ , 0.08 g of  $\text{MnCl}_2(\text{H}_2\text{O})_4$ , 1 ml of OAm, 1 ml of OA, and 5 ml of ODE were added to a 25-mL three-neck flask and dried in a vacuum at 120 °C for 1 h. And then, the flask was heated up to 180 °C under nitrogen. At this temperature, 0.5 mL of dried OAm and 0.5 mL of dried OA were subsequently injected to solubilize the Pb and Mn sources. Then, 0.4 mL of Cs-oleate was swiftly injected, and after 5 s, the solution was cooled with an ice bath. The QDs were precipitated with hexanes and ethyl acetate by the ratio of 1:3. Then, the solution was centrifuged at 5500 rpm for 5 min. After centrifugation, the precipitates were dispersed in toluene.

**Synthesis of Bi-doped  $\text{Cs}_2\text{SnCl}_6$**  The Bi-doped  $\text{Cs}_2\text{SnCl}_6$  was synthesized by hydrothermal reaction method. Typically, 0.337 g of  $\text{CsCl}$ , 0.189 g of  $\text{SnCl}_2$ , 0.032 g of  $\text{BiCl}_3$  powders, and 4.0 mL of 37% hydrochloric acid were sealed into a Teflon-lined autoclave (30 mL) and heated at 220 °C for 20 h. After the reaction, the autoclave was slowly cooled to room temperature, and a white crystal of Bi-doped  $\text{Cs}_2\text{SnCl}_6$  could be separated by centrifugation (3000 rpm, 2 min).

**Fabrication of LED Devices** UV-LED chips with an emission peak wavelength centered at 365 nm were purchased from Shine On Corp. In a typical preparation, a certain amount of Bi-doped  $\text{Cs}_2\text{SnCl}_6$  powder was mixed with PMMA/toluene solution and coated onto the UV-LED chip. Next, Mn-Doped  $\text{CsPbCl}_3$  QD solution was added into a 1-ml transparent PMMA/toluene solution. After that, the Mn-doped  $\text{CsPbCl}_3$  solution was coated onto the UV-LED chip which was already coated with Bi-doped  $\text{Cs}_2\text{SnCl}_6$ . The device was then cured at room temperature for 30 min.

**Measurement and Characterization** Fluorescence emission spectra were conducted on an Ocean Optics spectrometer. Absorbance spectra of samples were measured by using a Shimadzu UV-2550 spectrophotometer. For Bi-doped  $\text{Cs}_2\text{SnCl}_6$  diffuse reflectance (R) spectra were measured by Ocean Optics spectrometer, and the Abs coefficient  $\alpha$  was obtained by using the Kubelka–Munk theory  $(1 - R) \times (1 - R) / 2R$ . The excitation spectra and time-resolved PL spectroscopy (TRPL) have been measured by an Edinburgh FLS920 fluorescence

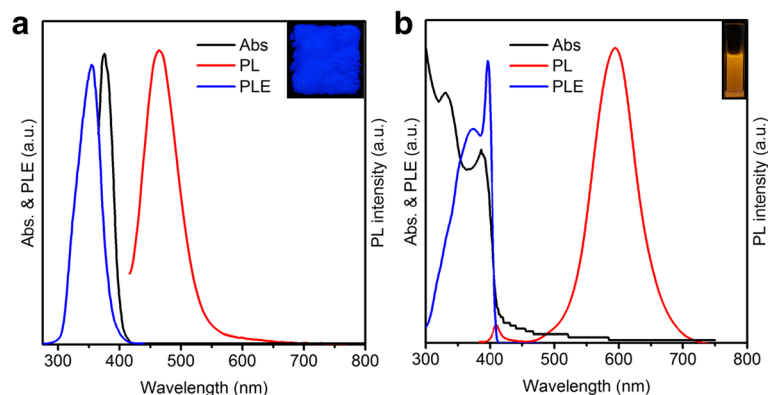


**Fig. 1** **a** Abs, PL, and PLE spectra of Bi-doped  $\text{Cs}_2\text{SnCl}_6$  QDs. The inset is the photograph of the sample under UV excitation. **b** Abs, PL, and PLE spectra of Mn-doped  $\text{CsPbCl}_3$  QDs. The inset is the photograph of the sample under UV excitation

spectrometer. The morphology of the QDs was acquired by a FEI Tecnai G2 Spirit TWIN transmission electron microscope (TEM) operating at 100 kV. Scanning electron microscope (SEM) and energy-dispersive X-ray spectroscopy (EDX) measurement have been performed by Quanta 450 FEG. X-ray diffraction (XRD) patterns of perovskites were carried out using a Bruker D8 Advance X-ray diffractometer (Cu  $K\alpha$ :  $\lambda = 1.5406 \text{ \AA}$ ). The absolute PL QYs of the samples were obtained by a fluorescence spectrometer (FLS920P, Edinburgh Instruments) equipped with an integrating sphere with its inner face coated with BENFLEC. The brightness and efficiency have been measured by ATA-1000 electroluminescence measurement system (Everfine in People's Republic of China).

## Results and Discussion

Bi-doped  $\text{Cs}_2\text{SnCl}_6$  perovskite was synthesized according to the previous approach with little modification [33]. The Abs and PL spectra of Bi-doped  $\text{Cs}_2\text{SnCl}_6$  are presented in Fig. 1a. As shown in Fig. 1a, the sharp Abs peak at around 375 nm could be assigned to the transitions from the defect band (caused by Bi doping) to the host conduction band minimum, which is in good accordance with previous reports [33]. The XRD pattern

also indicates the formation of Sn-based perovskite (Fig. 3a). All the diffraction peaks matched well with the  $\text{Cs}_2\text{SnCl}_6$  crystal structure (ICSD #9023), and no impurity phases were detected, which is in good accordance with a previous report [33]. The Bi-doped  $\text{Cs}_2\text{SnCl}_6$  can be excited by UV light (365 nm) and exhibits bright blue light with the PL emission peak located at 465 nm (Fig. 1a). The full width at half maximum (FWHM) of Bi-doped  $\text{Cs}_2\text{SnCl}_6$  is 65 nm, and the QY of Bi-doped  $\text{Cs}_2\text{SnCl}_6$  is up to 76%. The PL excitation (PLE) spectrum of Bi-doped  $\text{Cs}_2\text{SnCl}_6$  has been measured (detected at 465 nm) and shown in Fig. 1a. A broad peak located at 350 nm can be observed in the PLE spectrum of Bi-doped  $\text{Cs}_2\text{SnCl}_6$ , which shifts slightly compared to the Abs spectrum. The similar variation was observed by a previous report [33]. In addition, this Bi-doped  $\text{Cs}_2\text{SnCl}_6$  shows excellent stability. After being irradiated for 300 h with UV light, the PL intensity is nearly constant. The perovskite powder can maintain its QY after being exposed to air for 3 months (25 °C, relative humidity 35–50%).

Mn-doped  $\text{CsPbCl}_3$  QDs were prepared according to an established process with minor modification [32]. As shown in Fig. 1b, the Abs peak at around 400 nm is

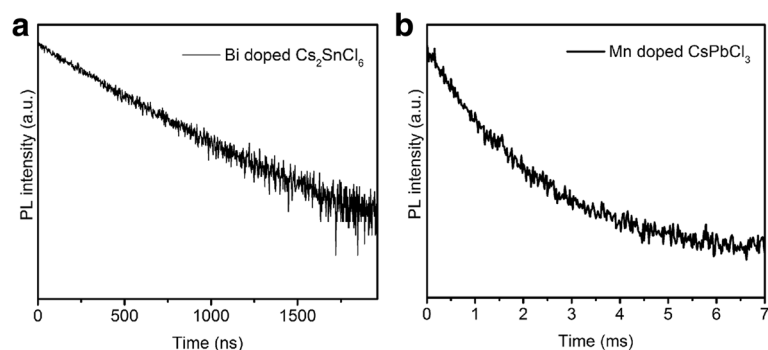
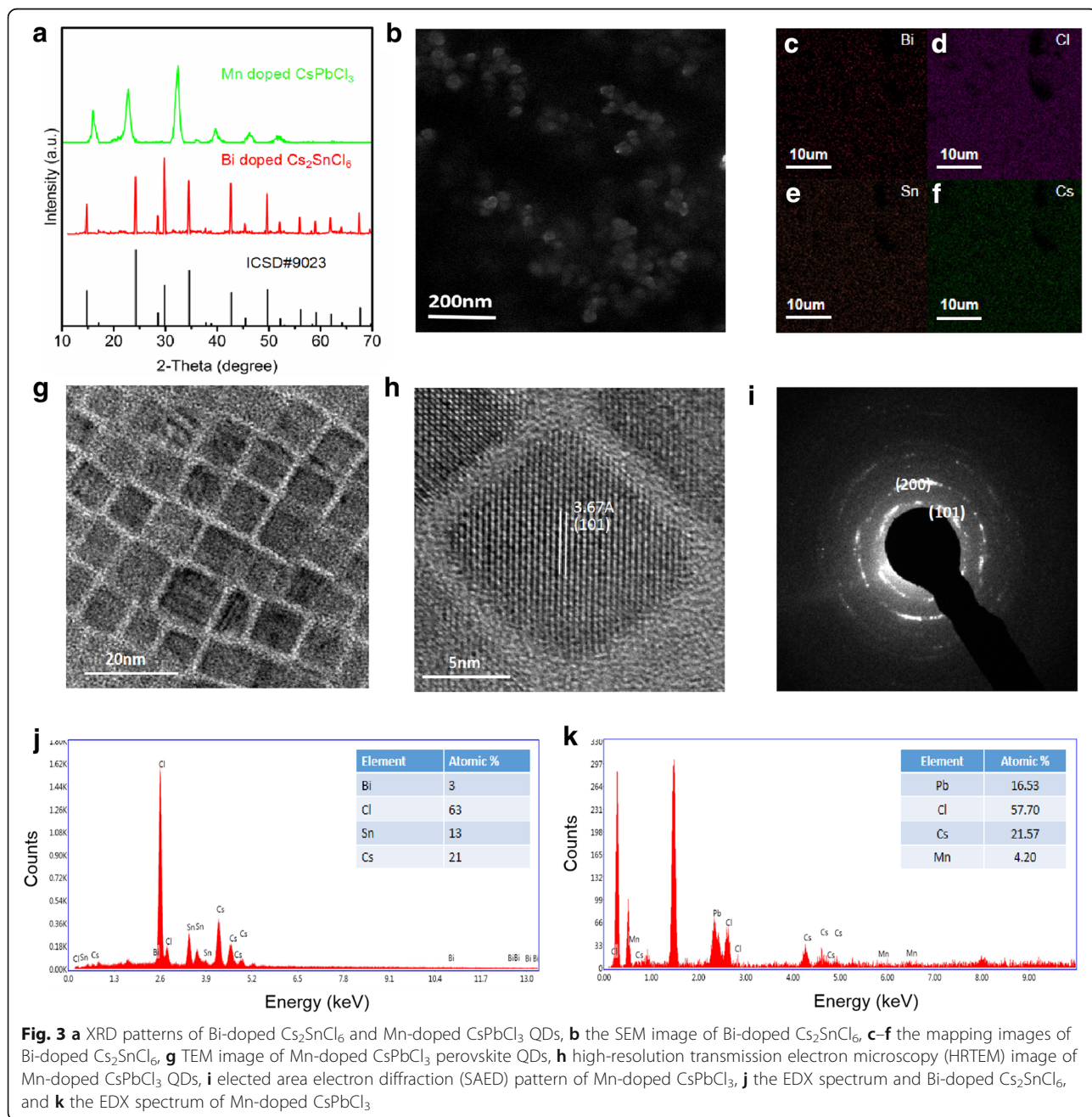


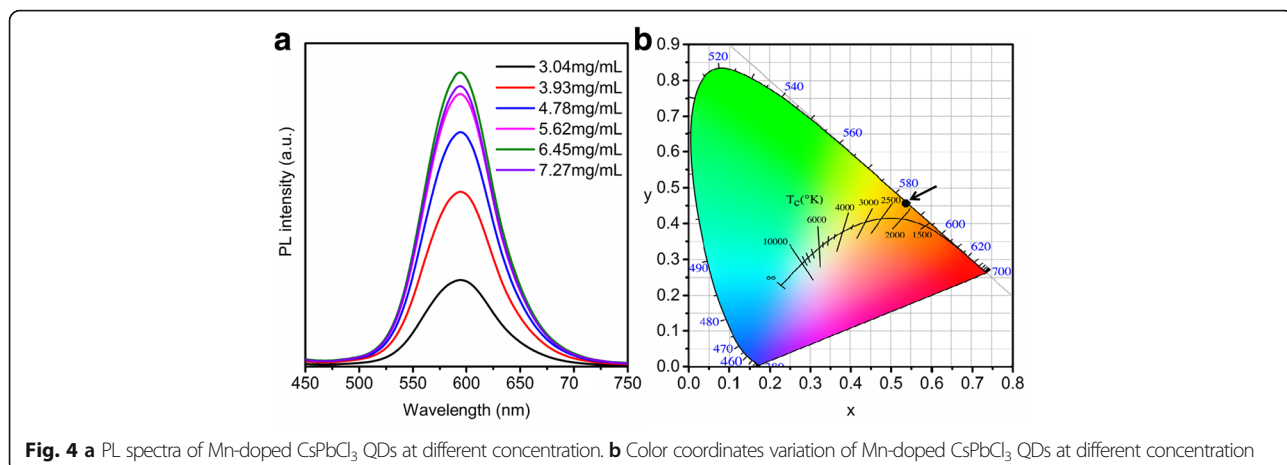
**Fig. 2** **a** PL decay and fitted curves of Bi-doped  $\text{Cs}_2\text{SnCl}_6$ . **b** PL decay and fitted curves of Mn-doped  $\text{CsPbCl}_3$

observed, which is assigned to exciton Abs of CsPbCl<sub>3</sub>. Under UV light (365 nm), the QD solution shows a bright orange emission (Fig. 1b, inset). Two peaks are observed in the PL emission spectrum, which center at 405 nm and 595 nm, respectively (Fig. 1b). The peak at 405 nm is assigned to the CsPbCl<sub>3</sub> host, while the broad emission band with the FWHM at about 80 nm is assigned to Mn<sup>2+</sup> d-d emission [31, 34]. The QY of our product is reaching to 52%, which is comparable with other reports [32, 35, 36]. The PLE spectrum of Mn-doped CsPbCl<sub>3</sub> has been measured (detected at 595 nm) and shown in Fig. 1b. The PLE spectrum of

Mn-doped CsPbCl<sub>3</sub> closely follows the Abs spectrum, which demonstrates that the strong PL peak of the Mn emission originates from the exciton of perovskite. The as-prepared QDs show excellent stability, which can preserve their emission properties under ambient atmospheres for at least 3 months (25 °C, relative humidity 35–50%).

The PL lifetimes of Bi-doped Cs<sub>2</sub>SnCl<sub>6</sub> and Mn-doped CsPbCl<sub>3</sub> were measured using TRPL. As shown in Fig. 2a, the decay curve of Bi-doped Cs<sub>2</sub>SnCl<sub>6</sub> is fitted well by an exponential function and the lifetime is 375 ns, which is in good accordance with the previous report

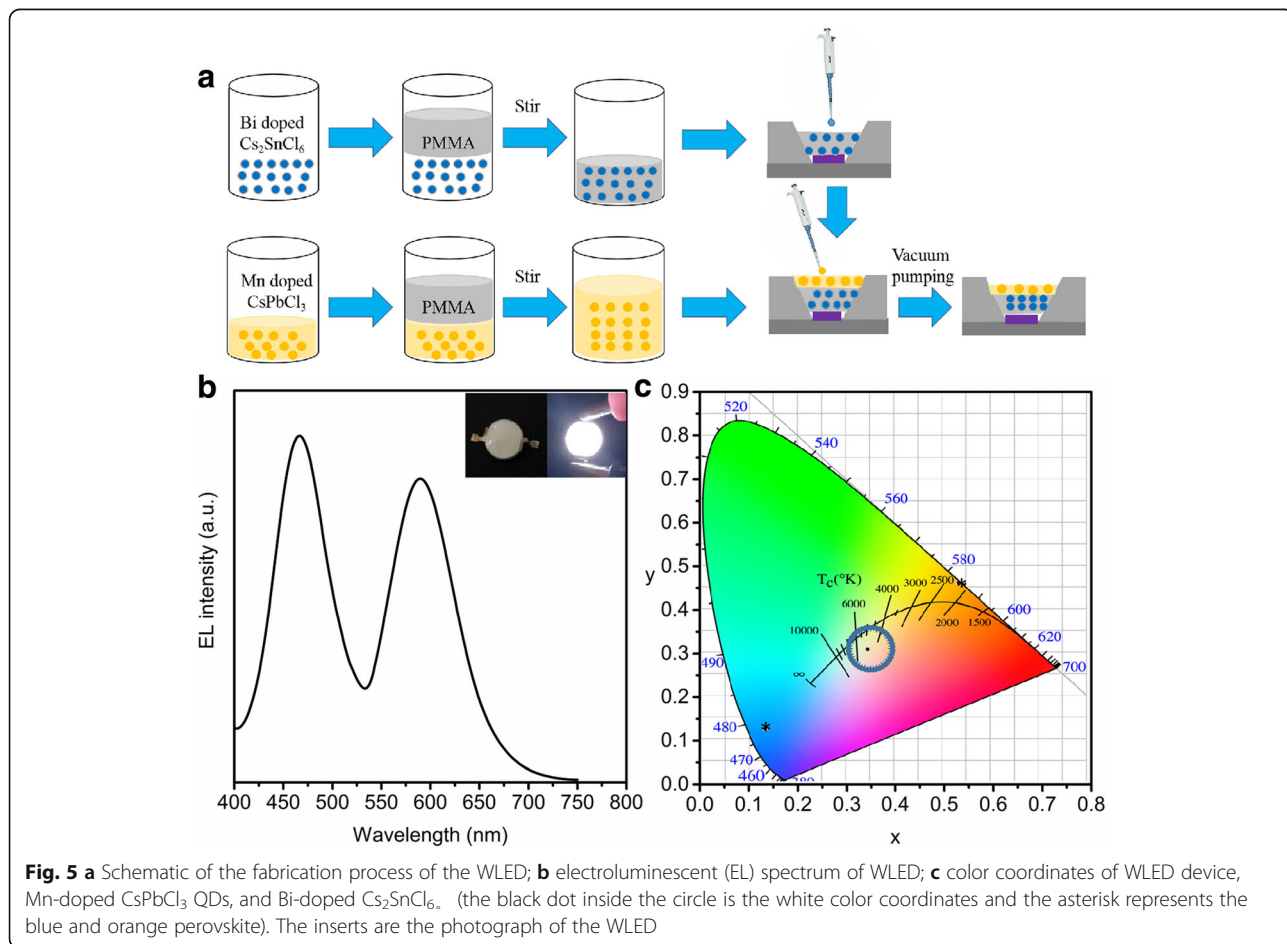




[33]. As for Mn-doped CsPbCl<sub>3</sub> QDs, the lifetime is longer (1.7 ms), which supports that it originates from the spin-forbidden ligand field transition of the Mn<sup>2+</sup> ions [32].

Figure 3b shows the SEM image of Bi-doped Cs<sub>2</sub>SnCl<sub>6</sub> perovskite. The spherical Bi-doped Cs<sub>2</sub>SnCl<sub>6</sub> perovskite with a diameter of 53 nm can be observed. EDX and

mapping images further confirm the presence of Bi in Cs<sub>2</sub>SnCl<sub>6</sub> (Fig. 3j, c–f). The ratio of Cs, Sn, Bi, and Cl is 1:0.62:0.14:3, which is in good accordance with other reports [33]. Figure 3g shows the TEM image of Mn-doped CsPbCl<sub>3</sub> QDs. As can be seen, the Mn-doped CsPbCl<sub>3</sub> QDs show a cubic morphology with an average size of ~12 nm. As can be seen from Fig. 3k, the ratio of



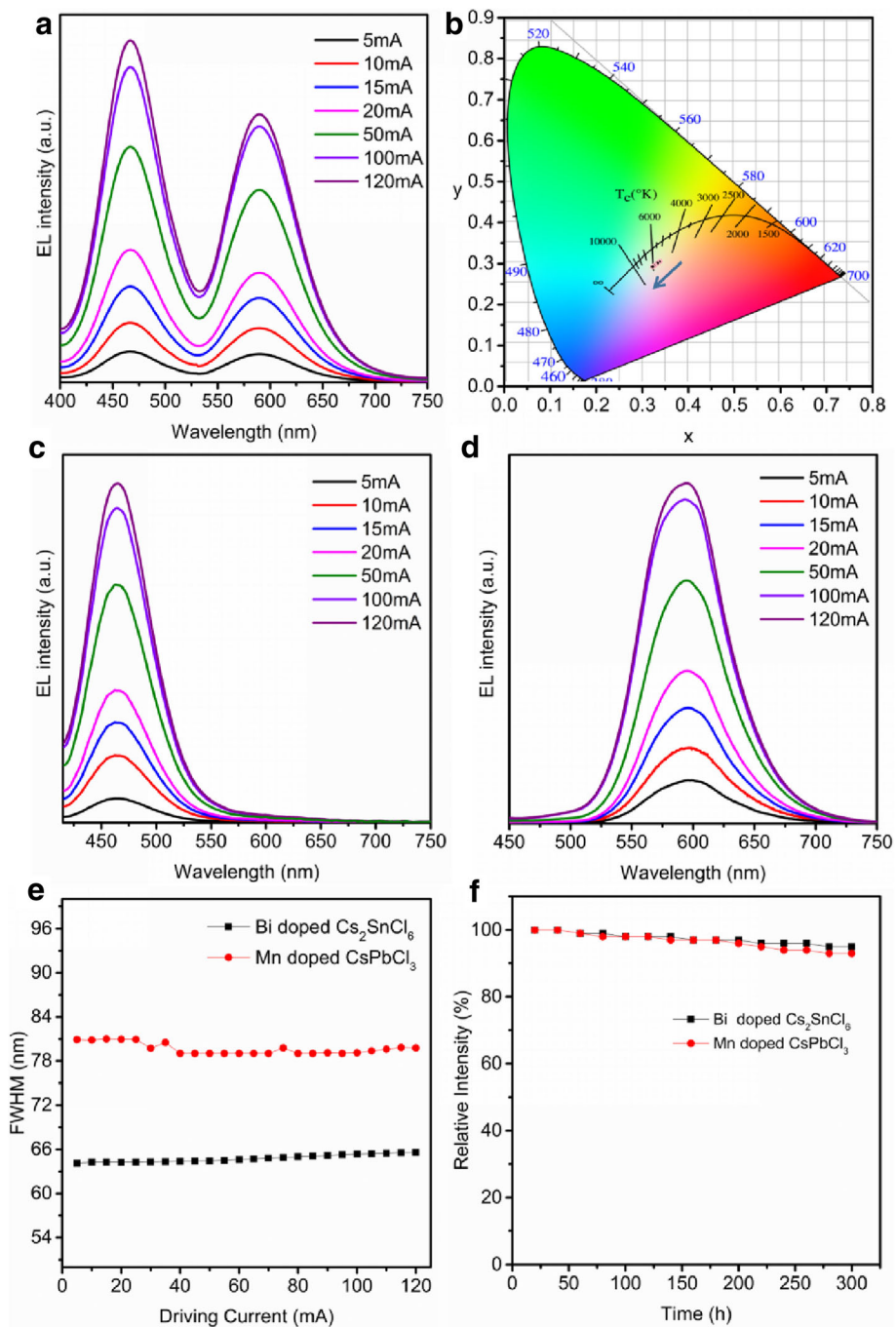


**Fig. 6** **a** PL spectra of WLED device under different injection currents, **b** chromaticity coordinates change of WLED device under different injection currents, **c** PL spectra of Bi-doped  $\text{Cs}_2\text{SnCl}_6$  LED device under different injection currents, **d** PL spectra of Mn-doped  $\text{CsPbCl}_3$  LED device under different injection currents, **e** the FWHM variation of Bi-doped  $\text{Cs}_2\text{SnCl}_6$  and Mn-doped  $\text{CsPbCl}_3$ , **f** the PL intensity variation measured at different working time intervals

Cs, Pb, Mn, and Cl is 1:0.77:0.19:2.68. The HRTEM image displays the lattice fringes of the Mn-doped  $\text{CsPbCl}_3$  QDs, which shows an interplanar distance of 3.67 Å, and matches well with that of the (101) plane (Fig. 3h). The SAED pattern is shown in Fig. 4c. We can see that the QDs possess a tetragonal crystal structure

with corresponding (101) and (200) planes (Fig. 3i) [31]. XRD pattern of the Mn-doped  $\text{CsPbCl}_3$  QDs shows that the diffraction peaks are corresponding to the tetragonal phase, which is consistent with the SAED results.

In order to acquire the optimal Mn doping concentration, the emission peak and FWHM variation are

**Table 1** Color coordinates ( $x$ ,  $y$ ), CCT, and  $R_a$  of the WLED device under different injection currents

Current (mA)	$x$	$y$	CCT	$R_a$
5	0.340	0.301	5046	82
10	0.339	0.300	5095	81
15	0.334	0.297	5311	80
20	0.329	0.292	5700	79
50	0.328	0.291	5815	78
100	0.327	0.290	5849	78
120	0.324	0.288	6119	77

analyzed and shown in Fig. 4. It can be seen from Fig. 4a that the PL intensity increases as the concentration of  $\text{Mn}^{2+}$  is increased from 3.04 to 6.45 mg/mL. Further increasing the  $\text{Mn}^{2+}$  concentration makes the PL intensity decrease, which is due to the self-Abs effect at high concentration. During the whole process, the PL peak position and the FWHM remains the same. In other words, the change of  $\text{Mn}^{2+}$  concentration has no effect on the PL emission peak and FWHM, which are also verified by the color coordinates chart (Fig. 4b). No matter how the concentration changes, the color coordinates are basically maintained at (0.535, 0.460) (the black dots). Therefore, the concentration of 6.45 mg/mL is taken as the optimal concentration.

A WLED was fabricated by coating blue-emitting Bi-doped  $\text{Cs}_2\text{SnCl}_6$  powder and orange-emitting Mn-doped  $\text{CsPbCl}_3$  QDs onto a commercially available 365 nm LED chip (Fig. 5a). As shown in Fig. 5b, two obvious peaks can be seen from the EL spectrum of the WLED, which attribute to Bi-doped  $\text{Cs}_2\text{SnCl}_6$  and

Mn-doped  $\text{CsPbCl}_3$ . The perseverance of these two peaks indicates that no anion exchange and other chemical reactions occur in the fabrication process. In bright white light with color coordinates of (0.334, 0.297), the correlated color temperature of 5311 K can be observed when the WLED is operated at 15 mA (Fig. 5b and c). The highest luminous efficiency and luminance of the WLED reach up to 20.8 lm/W and 78,000  $\text{cd m}^{-2}$ , respectively, which are comparable with other UV chip-based WLEDs [4, 37–39].

The emission spectra of the as-fabricated WLED with the driving currents of 5 mA–120 mA are given in Fig. 6a. The detailed characteristics including color coordinates, CCT, and CRI of the as-fabricated WLED are shown in Table 1. As shown in Fig. 6a, the EL intensities of both peaks increase gradually along with increasing the current and show no saturation. Besides, no obvious shift of the peak position for the EL spectrum occurred under different injection currents. Color coordinates of these PL spectra are shown in Fig. 6b. The chromaticity coordinates show little shift ( $x < 0.02$ ,  $y < 0.02$ ) to the left with increasing the driving currents. We can observe that the EL intensity of Bi-doped  $\text{Cs}_2\text{SnCl}_6$  increases faster than that of the Mn-doped  $\text{CsPbCl}_3$ , which can result in chromaticity coordinates moving left. However, the FWHM variation and the shift of emission peak also cause chromaticity coordinates to move. As we discussed above, the emission peak is unchanged with the increase of currents. Because of their broad FWHM, the emission peaks of Bi-doped  $\text{Cs}_2\text{SnCl}_6$  and Mn-doped  $\text{CsPbCl}_3$  overlap, which is difficult to analyze the FWHM variation. Therefore, monochromatic LEDs have been fabricated to analyze each FWHM variation. Figure 6c

**Table 2** Comparison of different WLEDs fabricated by perovskite

Ref.	LED chip	Red component	Green component	Blue component	PL intensity, working time	Current (mA)
1	Blue LED	$\text{CsPb (Br/I)}_3$	$\text{CsPbBr}_3$	Blue LED	10 h, 83%	20
2	UV LED	2.7% Ce/9.1% Mn co-doped $\text{CsPbCl}_{1.8}\text{Br}_{1.2}$		UV LED	20 h, 89%	15
3	Blue LED	$\text{Mn}^{2+}$ -doped $\text{CsPb (Cl}_{0.5}\text{Br}_{0.5})_3$	$\text{CsPbBr}_3$	Blue LED	24 h, 96%	20
4	UV LED	$\text{CsPb (Br}_{0.4}\text{I}_{0.6})_3$	$\text{CsPb (Br}_{0.8}\text{I}_{0.2})_3$	UV LED	100 h, 73%	15
5	UV LED	$\text{CsPbI}_3$	$\text{CsPb (Br/I)}_3$	$\text{CsPbBr}_3$	30 h, 83.5%	15
6	Blue LED	CSAN:Eu <sup>2+</sup> -EC	$\text{CsPbBr}_3$ -EC	Blue LED	30 min, 80%	20
7	Blue LED	$\text{K}_2\text{SiF}_6$ :Mn <sup>4+</sup> phosphors	$\text{CsPbBr}_3$	Blue LED	13 h, 96%	6
8	Blue LED	$\text{CaAlSi}_3$ :Eu <sup>2+</sup>	$\text{CsPb}_{0.64}\text{Sn}_{0.36}\text{Br}_3$	Blue LED	50 h, 97%	15
This work	UV LED	Mn-doped $\text{CsPbCl}_3$	–	Bi-doped $\text{Cs}_2\text{SnCl}_6$	50 h, 99% 100 h, 97%	15

and d show the emission spectra of Bi-doped  $\text{Cs}_2\text{SnCl}_6$  and Mn-doped  $\text{CsPbCl}_3$  LEDs, respectively. In the wide current range from 5 to 120 mA, no shift of the PL emission peaks occurs, which is in good accordance with the WLED results (Fig. 6c and d). The FWHM variation of the coated LEDs under different currents is shown in Fig. 6e. As can be seen, the FWHMs of Bi-doped  $\text{Cs}_2\text{SnCl}_6$  and Mn-doped  $\text{CsPbCl}_3$  are nearly constant, indicating that the variation of chromaticity coordinates of the WLED only results from the change of intensity of the EL. The difference of EL intensity variation perhaps comes from the different thermal stability of Bi-doped  $\text{Cs}_2\text{SnCl}_6$  and Mn-doped  $\text{CsPbCl}_3$ , because the increase of currents could result in the temperature of LED chip increasing. This insignificant change can be further alleviated by adopting a remote-type LED structure. Moreover, the long-term operating stability can be observed from Fig. 6f. After a continuous work of 300 h, the EL intensities of both Bi-doped  $\text{Cs}_2\text{SnCl}_6$  and Mn-doped  $\text{CsPbCl}_3$  are declined less than 10%. Actually, the half-life of the WLED is 3000 h, which is far better than I-containing perovskites [15, 17, 18, 40]. As can be seen from Table 2, after the as-prepared WLED continues working at 15 mA over 50 h, the PL intensity drops to 99% of the original, which is much better than other reports [17, 18, 36, 40–44]. After working 100 hours, the PL intensity only drops to 97%.

Nowadays, perovskite heterojunctions have been adopted to improve the physical properties of perovskite [45, 46]. Usually, these heterojunctions can integrate the merits of both materials, such as perovskite-polymer bulk heterostructure, perovskite-PbS core-shell structure, and perovskite-plasmonic Au or Ag composite material [47–49], which can enhance efficiency. However, due to the poor stability of perovskite, it is difficult to design and fabricate heterojunction. Besides, these perovskite heterojunctions may be not stable compared to pure perovskite.

## Conclusion

In conclusion, we have combined high-quality blue-emitting bismuth-doped  $\text{Cs}_2\text{SnCl}_6$  perovskite with orange-emitting Mn-doped  $\text{CsPbCl}_3$  QDs to fabricate WLED. Because they all contain the same anion of Cl, anion exchange reaction can be avoided. Besides, orange-emitting Mn-doped  $\text{CsPbCl}_3$  QDs show better stability compared with iodine-containing counterparts. The WLED with color coordinates of (0.334, 0.297) is acquired by tuning the ratio of them. In addition, the WLED show excellent long-term operating stability, which is by far, to our knowledge, the most stable one among perovskite-based WLEDs. We believe our findings will open up new avenues for the exploration of novel lead-free perovskite-based WLED.

## Abbreviations

QDs: Quantum dots; WLEDs: White light-emitting diodes; QY: Quantum yield; PCE: Power conversion efficiency; PL: Photoluminescence;  $\text{Cs}_2\text{CO}_3$ : Cesium carbonate;  $\text{PbCl}_2$ : Lead (II) chloride;  $\text{CsCl}$ : Cesium chloride; OA: Oleic acid; ODE: 1-Octadecene;  $\text{MnCl}_2(\text{H}_2\text{O})_4$ : Manganese chloride tetrahydrate; OAm: Oleylamine;  $\text{SnCl}_2$ : Tin chloride;  $\text{BiCl}_3$ : Bismuth chloride; PMMA: Polymethyl methacrylate; HCl: Hydrochloric acid; TRPL: Time-resolved PL spectroscopy; TEM: Transmission electron microscope; SEM: Scanning electron microscope; EDX: Energy dispersive X-ray detector; XRD: X-ray diffraction; PLE: PL excitation; FWHM: Full width at half maximum; EL: Electroluminescent; HRTEM: High-resolution transmission electron microscopy; SAED: Selected area electron diffraction

## Acknowledgements

This study was supported by the Natural Science Foundation of Hebei Province (F2018202046) and State Key Laboratory of Reliability and Intelligence of Electrical Equipment (EERIZZ2018003).

## Funding

This study was funded by the Natural Science Foundation of Hebei Province (F2018202046) and State Key Laboratory of Reliability and Intelligence of Electrical Equipment (EERIZZ2018003).

## Availability of Data and Materials

The datasets generated during and/or analyzed during the current study are available from the corresponding authors on reasonable request.

## Authors' Contributions

HL, CS, and WB conceived and designed the experiments. HL performed the experiments and analyzed the data. ZG, CG, SS, LW, and SS contributed to the analysis tools. HL and CS wrote the manuscript. All authors read and approved the final manuscript.

## Competing Interests

The authors declare that they have no competing interests.

## Publisher's Note

Springer Nature remains neutral with regard to jurisdictional claims in published maps and institutional affiliations.

Received: 30 January 2019 Accepted: 14 April 2019

Published online: 02 May 2019

## References

- Schubert EF, Kim JK (2005) Solid-state light sources getting smart. *Science* 308:1274–1278
- Chen LY, Chang JK, Cheng WC et al (2015) Chromaticity tailorable glass-based phosphor-converted white light-emitting diodes with high color rendering index. *Opt Express* 23:A1024–A1029
- Chen KJ, Lai YC, Lin BC et al (2015) Efficient hybrid white light-emitting diodes by organic-inorganic materials at different CCT from 3000 K to 9000 K. *Opt Express* 23:A204–A210
- Gao Z, Sun C, Liu H et al (2019) White light-emitting diodes based on carbon dots and Mn-doped  $\text{CsPb}_x\text{Mn}_{1-x}\text{Cl}_3$  nanocrystals. *Nanotechnology* 30:245201–245205
- Lan C, Zhou Z, Wei R et al (2019) Two-dimensional perovskite materials: from synthesis to energy-related applications. *Materials today energy* 11:61–82
- Al-Amri AM, Cheng B, He J-H et al (2019) Perovskite methylammonium lead trihalide heterostructures: progress and challenges. *IEEE Trans Nano* 18:1–12
- Zhao D, Wang C, Song Z et al (2018) Four-terminal all-perovskite tandem solar cells achieving power conversion efficiencies exceeding 23%. *ACS Energy Lett* 3:305–306
- Zhang Y, Xu W, Xu X et al (2019) Self-powered dual-color UV-green photodetectors based on  $\text{SnO}_2$  millimeter wire and microwires/ $\text{CsPbBr}_3$  particle heterojunctions. *J Phys Chem Lett* 10:836–841
- Lin CH, Cheng B, Li TY et al (2019) Orthogonal lithography for halide perovskite optoelectronic nanodevices. *ACS Nano* 13:1168–1176
- Dong R, Lan C, Xu X et al (2018) A novel series of quasi-2D Ruddlesden-Popper perovskites based on short-chained spacer cation for enhanced photodetection. *ACS Appl Mater Inter* 10:19019–19026



11. Yakunin S, Protesescu L, Krie F et al (2015) Low-threshold amplified spontaneous emission and lasing from colloidal nanocrystals of caesium lead halide perovskites. *Nat Commun* 6:8056–8062
12. Protesescu L, Yakunin S, Bodnarchuk MI et al (2015) Nanocrystals of cesium lead halide perovskites (CsPbX<sub>3</sub>, X = Cl, Br, and I): novel optoelectronic materials showing bright emission with wide color gamut. *Nano Lett* 15: 3692–3696
13. Ramasamy P, Lim DH, Kim B et al (2016) All-inorganic cesium lead halide perovskite nanocrystals for photodetector applications. *Chem Commun* 52: 2067–2070
14. Bai S, Yuan Z, Gao F et al (2016) Colloidal metal halide perovskite nanocrystals: synthesis, characterization, and applications. *Mater Chem* 4:3898–3904
15. Sun C, Gao Z, Liu H et al (2018) A new method to discover the reaction mechanism of perovskite nanocrystals. *Dalton Trans* 47:16218–16224
16. Sun C, Su S, Gao Z et al (2019) Stimuli-responsive inks based on perovskite quantum dots for advanced full-color information encryption and decryption. *ACS Appl Mater Inter* 11:8210–8216
17. Sun C, Zhang Y, Ruan C et al (2016) Efficient and stable white LEDs with silica-coated inorganic perovskite quantum dots. *Adv Mater* 28:10088–10094
18. Shen X, Sun C, Bai X et al (2018) Efficient and stable CsPb (Br/I)<sub>3</sub>@anthracene composites for white light-emitting devices. *ACS Appl Mater Inter* 10:16768–16775
19. Zhou Q, Bai Z, Lu WG et al (2016) In situ fabrication of halide perovskite nanocrystal-embedded polymer composite films with enhanced photoluminescence for display backlights. *Adv Mater* 28:9163–9168
20. Chen YM, Zhou Y, Zhao Q et al (2018) Cs<sub>4</sub>PbBr<sub>6</sub>/CsPbBr<sub>3</sub> Perovskite composites with near-unity luminescence quantum yield: large-scale synthesis, luminescence and formation mechanism, and white light-emitting diode application. *ACS Appl Mater Inter* 10:15905–15912
21. Li X, Wu Y, Zhang S et al (2016) CsPbX<sub>3</sub> quantum dots for lighting and displays: room-temperature synthesis, photoluminescence superiorities, underlying origins and white light-emitting diodes. *Adv Funct Mater* 26: 2435–2445
22. Li Y, Lv Y, Guo Z et al (2018) One-step preparation of long-term stable and flexible CsPbBr<sub>3</sub> perovskite quantum dots/ethylene vinyl acetate copolymer composite films for white light-emitting diodes. *ACS Appl Mater Inter* 10: 15888–15894
23. Dohner ER, Jaffe A, Bradshaw LR et al (2014) Intrinsic white-light emission from layered hybrid perovskites. *J Am Chem Soc* 136:13154–13157
24. Yuan Z, Zhou C, Messier J et al (2016) A microscale perovskite as single component broadband phosphor for downconversion white-light-emitting devices. *Adv Opt Mater* 4:2009–2015
25. Thirumal K, Chong WK, Xie W et al (2017) Morphology-independent stable white-light emission from self-assembled two-dimensional perovskites driven by strong exciton–phonon coupling to the organic framework. *Chem Mater* 29:3947–3953
26. Wang A, Guo Y, Muhammad F et al (2017) Controlled synthesis of lead-free cesium tin halide perovskite cubic nanocages with high stability. *Chem Mater* 29:6493–6501
27. Zhu X (2016) The perovskite fever and beyond. *Acc Chem Res* 49:355–356
28. Swarnkar A, Ravi VK, Nag A et al (2017) Beyond colloidal cesium lead halide perovskite nanocrystals: analogous metal halides and doping. *ACS Energy Lett* 2:1089–1098
29. Stoumpos CC, Frazer L, Clark DJ et al (2015) Hybrid germanium iodide perovskite semiconductors: active lone pairs, structural distortions, direct and indirect energy gaps and strong nonlinear optical properties. *J Am Chem Soc* 137:6804–6819
30. McClure ET, Ball MR, Windl W et al (2016) Cs<sub>2</sub>AgBiX<sub>6</sub> (X = Br, Cl): new visible light absorbing, lead-free halide perovskite semiconductors. *Chem Mater* 28: 1348–1354
31. Liu H, Wu Z, Shao J et al (2017) CsPb<sub>1-x</sub>Mn<sub>x</sub>Cl<sub>3</sub> perovskite quantum dots with high Mn substitution ratio. *ACS Nano* 11:2239–2247
32. Parobek D, Roman BJ, Dong Y et al (2016) Exciton-to-dopant energy transfer in Mn-doped cesium lead halide perovskite nanocrystals. *Nano Lett* 16: 7376–7380
33. Tan Z, Li J, Zhang C et al (2018) Highly efficient blue-emitting Bi-doped Cs<sub>2</sub>SnCl<sub>6</sub> perovskite variant: photoluminescence induced by impurity doping. *Adv Funct Mater* 28:1801131–1801140
34. Liu W, Lin Q, Li H et al (2016) Mn<sup>2+</sup>-doped lead halide perovskite nanocrystals with dual-color emission controlled by halide content. *J Am Chem Soc* 138:14954–14961
35. Das AS, Dutta SK, Dutta A et al (2017) Chemically tailoring the dopant emission in manganese-doped CsPbCl<sub>3</sub> perovskite nanocrystals. *Angew Chem Int Ed* 56:8746–8750
36. Chen D, Fang G, Chen X et al (2017) Silica-coated Mn-doped CsPb (Cl/Br)<sub>3</sub> inorganic perovskite quantum dots: exciton-to-Mn energy transfer and blue-excitable solid-state lighting. *ACS Appl Mater Inter* 9:40477–40487
37. Tian Z, Zhang X, Li D et al (2017) Full-color inorganic carbon dot phosphors for white-light-emitting diodes. *Adv Opt Mater* 5:1700416–1700424
38. Zhu J, Bai X, Bai J et al (2018) Emitting color tunable carbon dots by adjusting solvent towards light-emitting devices. *Nanotechnology* 29: 085705–085712
39. Sun C, Zhang Y, Kalytchuk S et al (2015) Down-conversion monochromatic light-emitting diodes with the color determined by the active layer thickness and concentration of carbon dots. *J Mater Chem C* 3:6613–6615
40. Shao H, Bai X, Pan G et al (2018) Highly efficient and stable blue-emitting CsPbBr<sub>3</sub>@SiO<sub>2</sub> nanospheres through low temperature synthesis for nanoprinting and WLED. *Nanotechnology* 29:285706–285714
41. Pan G, Bai X, Xu W et al (2018) Impurity ions codoped cesium lead halide perovskite nanocrystals with bright white light emission toward ultraviolet-white light-emitting diode. *ACS Appl Mater Inter* 10:39040–39048
42. Zhang M, Wang M, Yang Z et al (2018) Preparation of all-inorganic perovskite quantum dots-polymer composite for white LEDs application. *J Alloy Compd* 748:537–545
43. Zhang F, Shi ZF, Ma ZZ et al (2018) Silica coating enhances the stability of inorganic perovskite nanocrystals for efficient and stable down-conversion in white light-emitting devices. *Nanoscale* 10:20131–20139
44. Liu S, Shao G, Ding L et al (2019) Sn-doped CsPbBr<sub>3</sub> QDs glasses with excellent stability and optical properties for WLED. *Chem Eng J* 361:937–944
45. Zhao B, Bai S, Kim V et al (2018) High-efficiency perovskite-polymer bulk heterostructure light-emitting diodes. *Nat Photonics* 12:783–789
46. Tang SY, Medina H, Yen YT et al (2019) Enhanced photocarrier generation with selectable wavelengths by M-decorated-CuInS<sub>2</sub> nanocrystals (M = Au and Pt) synthesized in a single surfactant process on MoS<sub>2</sub> bilayers. *Small* 15:1803529–1803537
47. Ye S, Y M, Yan W et al (2017) Enhanced photoluminescence of CsPbBr<sub>3</sub>@Ag hybrid perovskite quantum dots. *J Mater Chem C* 5:8187–8193
48. Zhang X, Lu M, Zhang Y et al (2018) PbS capped CsPbI<sub>3</sub> nanocrystals for efficient and stable light-emitting devices using p-i-n structures. *ACS Central Sci* 4:1352–1359
49. Shi Z, Li Y, Li S et al (2018) Localized surface plasmon enhanced all-inorganic perovskite quantum dot light-emitting diodes based on coaxial core/shell heterojunction architecture. *Adv Funct Mater* 28:1707031–1707041

Submit your manuscript to a SpringerOpen<sup>®</sup> journal and benefit from:

- Convenient online submission
- Rigorous peer review
- Open access: articles freely available online
- High visibility within the field
- Retaining the copyright to your article

Submit your next manuscript at ► [springeropen.com](https://www.springeropen.com)